

## A Low-Mass Neutron Flux Monitor for the *n*-TOF Facility at CERN

P. F. Mastinu<sup>1</sup>, U. Abbondanno<sup>1</sup>, G. Aerts<sup>2</sup>, H. Alvarez<sup>3</sup>, S. Andriamonje<sup>2</sup>, A. Angelopoulos<sup>4</sup>,  
P. Assimakopoulos<sup>5</sup>, C.O. Bacri<sup>6</sup>, G. Badurek<sup>7</sup>, P. Baumann<sup>8</sup>, F. Bečvář<sup>9</sup>, H. Beer<sup>10</sup>, J. Benlliure<sup>3</sup>,  
B. Berthier<sup>6</sup>, E. Berthomieux<sup>2</sup>, S. Boffi<sup>11</sup>, C. Borcea<sup>12</sup>, E. Boscolo-Marchi<sup>13</sup>, N. Bustreo<sup>13</sup>, P. Calviño<sup>14</sup>,  
D. Cano-Ott<sup>15</sup>, R. Capote<sup>15</sup>, P. Carlson<sup>17</sup>, P. Cennini<sup>12</sup>, V. Chepel<sup>18</sup>, E. Chiaveri<sup>12</sup>, C. Coceva<sup>19</sup>,  
N. Colonna<sup>20</sup>, G. Cortes<sup>14</sup>, D. Cortina<sup>3</sup>, A. Couture<sup>21</sup>, J. Cox<sup>21</sup>, S. Dababneh<sup>22</sup>, M. Dahlfors<sup>12</sup>, S. David<sup>6</sup>,  
R. Dolfini<sup>11</sup>, C. Domingo-Pardo<sup>23</sup>, I. Duran<sup>3</sup>, C. Eleftheriadis<sup>24</sup>, M. Embid-Segura<sup>15</sup>, L. Ferrant<sup>6</sup>,  
A. Ferrari<sup>12</sup>, L. Ferreira-Lourenco<sup>25</sup>, R. Ferreira-Marques<sup>18</sup>, H. Fraiss-Koelbl<sup>26</sup>, W.I. Furman<sup>27</sup>,  
Y. Giomataris<sup>2</sup>, I.F. Goncalves<sup>25</sup>, E. Gonzalez-Romero<sup>15</sup>, A. Goverdovski<sup>28</sup>, F. Gramegna<sup>13</sup>,  
E. Griesmayer<sup>26</sup>, F. Gunsing<sup>2</sup>, R. Haight<sup>29</sup>, M. Heil<sup>22</sup>, A. Herrera-Martinez<sup>12</sup>, K.G. Ioannides<sup>5</sup>,  
N. Janeva<sup>30</sup>, E. Jericha<sup>7</sup>, F. Käppeler<sup>10</sup>, Y. Kadi<sup>12</sup>, D. Karamanis<sup>5</sup>, A. Kelic<sup>8</sup>, V. Ketlerov<sup>28</sup>,  
G. Kitis<sup>24</sup>, P.E. Koehler<sup>31</sup>, V. Konovalov<sup>27</sup>, E. Kossionides<sup>32</sup>, V. Lacoste<sup>12</sup>, H. Leeb<sup>7</sup>, A. Lindote<sup>18</sup>,  
M.I. Lopes<sup>18</sup>, M. Loriggiola<sup>13</sup>, M. Lozano<sup>16</sup>, S. Lukic<sup>8</sup>, S. Markov<sup>30</sup>, S. Marigo<sup>13</sup>, S. Marrone<sup>20</sup>,  
J. Martinez-Val<sup>33</sup>, A. Mengoni<sup>12</sup>, P.M. Milazzo<sup>1</sup>, E. Minguez<sup>33</sup>, A. Molina-Coballes<sup>16</sup>, C. Moreau<sup>1</sup>,  
F. Neves<sup>18</sup>, H. Oberhummer<sup>7</sup>, S. O'Brien<sup>21</sup>, J. Pancin<sup>2</sup>, T. Papaevangelou<sup>24</sup>, C. Paradela<sup>3</sup>, A. Pavlik<sup>34</sup>,  
P. Pavlopoulos<sup>35</sup>, A. Perez-Parra<sup>15</sup>, J.M. Perlado<sup>33</sup>, L. Perrot<sup>2</sup>, V. Peskov<sup>17</sup>, R. Plag<sup>10</sup>, A. Plompen<sup>36</sup>,  
A. Plukis<sup>2</sup>, A. Poch<sup>14</sup>, A. Policarpo<sup>18</sup>, C. Pretel<sup>14</sup>, J.M. Quesada<sup>16</sup>, M. Radici<sup>11</sup>, S. Raman<sup>31</sup>, W. Rapp<sup>10</sup>,  
T. Rauscher<sup>35</sup>, R. Reifarth<sup>29</sup>, F. Rejmund<sup>6</sup>, M. Rosetti<sup>19</sup>, C. Rubbia<sup>11</sup>, G. Rudolf<sup>8</sup>, P. Rullhusen<sup>36</sup>,  
J. Salgado<sup>25</sup>, E. Savvidis<sup>24</sup>, J.C. Soares<sup>25</sup>, C. Stephan<sup>6</sup>, G. Tagliente<sup>20</sup>, J.L. Tain<sup>23</sup>, C. Tapia<sup>14</sup>,  
L. Tassan-Got<sup>6</sup>, L.M.N. Tavora<sup>25</sup>, R. Terlizzi<sup>20</sup>, M. Terrani<sup>11</sup>, N. Tsangas<sup>37</sup>, G. Vannini<sup>38</sup>, P. Vaz<sup>25</sup>,  
A. Ventura<sup>19</sup>, D. Villamarin-Fernandez<sup>15</sup>, M. Vincente-Vincente<sup>15</sup>, V. Vlachoudis<sup>12</sup>, R. Vlastou<sup>11</sup>,  
F. Voss<sup>10</sup>, H. Wendler<sup>12</sup>, M. Wiescher<sup>21</sup>, K. Wisshak<sup>10</sup>, and L. Zanini<sup>12</sup>

(The *n*-TOF Collaboration)

<sup>1</sup>*Instituto Nazionale di Fisica Nucleare-Sezione di Trieste, Italy;* <sup>2</sup>*CEA/Saclay - DSM/DAPNIA/SPhN, Gif-sur-Yvette, France*

<sup>3</sup>*Universidade de Santiago de Compostela, Spain;* <sup>4</sup>*Astro-Particle Consortium, University of Athens, Greece*

<sup>5</sup>*Astro-Particle Consortium, University of Ioannina, Greece;* <sup>6</sup>*Centre National de la Recherche Scientifique/IN2P3 - IPN, Orsay, France*

<sup>7</sup>*Atominstytut der Österreichischen Universitäten, Technische Universität Wien, Austria*

<sup>8</sup>*Centre National de la Recherche Scientifique/IN2P3 - IreS, Strasbourg, France;* <sup>9</sup>*Charles University, Prague, Czech Republic*

<sup>10</sup>*Forschungszentrum Karlsruhe GmbH;* <sup>11</sup>*Università degli Studi Pavia, Italy;* <sup>12</sup>*CERN, Geneva, Switzerland*

<sup>13</sup>*Instituto Nazionale di Fisica Nucleare, Laboratori Nazionali di Legnaro, Italy;* <sup>14</sup>*Universitat Politècnica de Catalunya, Barcelona, Spain*

<sup>15</sup>*Centro de Investigaciones Energéticas Medioambientales y Tecnológicas, Madrid, Spain*

<sup>16</sup>*Universidad de Sevilla, Spain;* <sup>17</sup>*Kungliga Tekniska Hogskolan, Physics Department, Stockholm, Sweden*

<sup>18</sup>*Laboratorio de Instrumentacao e Phisica Experimental de Particulas, Coimbra, Portugal;* <sup>19</sup>*ENEA, Bologna, Italy*

<sup>20</sup>*Instituto Nazionale di Fisica Nucleare-Sezione di Bari, Italy;* <sup>21</sup>*University of Notre Dame, USA*

<sup>22</sup>*Forschungszentrum Karlsruhe GmbH,* <sup>23</sup>*Instituto de Física Corpuscular, CSIC-Univ. Valencia, Spain*

<sup>24</sup>*Astro-Particle Consortium, University of Thessaloniki, Greece*

<sup>25</sup>*Instituto Tecnológico e Nuclear, Lisboa, Portugal;* <sup>26</sup>*Fachhochschule Wiener Neustadt, Wien, Austria*

<sup>27</sup>*Joint Institute for Nuclear Research, Frank Laboratory of Neutron Physics, Dubna, Russia*

<sup>28</sup>*Institute of Physics and Power Engineering, Obninsk, Russia;* <sup>29</sup>*Los Alamos National Laboratory, New Mexico, USA*

<sup>30</sup>*Institute for Nuclear Research and Nuclear Energy, Sofia, Bulgaria;* <sup>31</sup>*Oak Ridge National Laboratory, Physics Division, Oak Ridge, USA*

<sup>32</sup>*Astro-Particle Consortium, NCSR "Demokritos", Athens, Greece;* <sup>33</sup>*Universidad Politècnica de Madrid, Spain*

<sup>34</sup>*Institut für Isotopenforschung und Kernphysik, Universität Wien, Austria;* <sup>35</sup>*University of Basel, Switzerland*

<sup>36</sup>*CEC-JRC-IRMM, Geel, Belgium;* <sup>37</sup>*Astro-Particle Consortium, University of Thrace, Greece*

<sup>38</sup>*Dipartimento di Fisica and INFN, Bologna, Italy*

Received on 7 October, 2003

A small-mass system has been developed for monitoring the flux of neutrons with energy up to 1 MeV at the new time-of-flight facility at CERN, *n\_TOF*. The monitor is based on a thin Mylar foil with a  ${}^6\text{Li}$  deposit, placed in the neutron beam, and an array of Silicon detectors, placed outside the beam, for detecting the products of the  ${}^6\text{Li}(n, \alpha){}^3\text{H}$  reaction. The small amount of material on the beam ensures a minimal perturbation of the flux and minimizes the background related to scattered neutrons. Moreover, a further reduction of the  $\gamma$ -ray background has been obtained by constructing the scattering chamber hosting the device in carbon fibre. A detailed description of the flux monitor is here presented, together with the characteristics of the device, in terms of efficiency, resolution and induced background. The use of the monitor in the measurement of neutron capture cross-sections at *n\_TOF* is discussed

## 1 Introduction

In the last few years, new ideas and development in the field of nuclear technologies has led to a renewed interest in neutron cross-section data. The need for new measurements on a variety of isotopes is mainly related to the development of innovative systems for energy production and for nuclear waste incineration [1, 2, 3]. In particular, nuclear data are necessary for the feasibility study, and eventually for the design and construction of Accelerator Driven Systems. Cross-sections for neutron capture and fission-induced reactions are needed for the isotopes involved in the Thorium- Uranium fuel cycle, as well as for many long-lived fission fragments and actinides that constitute most of the high radiotoxic nuclear waste. Neutron capture data are also needed for many specific isotopes to address questions in Nuclear Astrophysics [4] that are still pending. With the aim of allowing new, accurate measurements of neutron cross-sections, an innovative neutron time-of-flight facility, *n\_TOF* [5], has recently been constructed at CERN. At *n\_TOF*, neutrons are produced by spallation of 20 GeV/c protons from the PS accelerator impinging onto a Pb block surrounded by a 5cm water layer acting as refrigerator and as moderator. An experimental area is currently located at the end of a 200m long time-of-flight tunnel hosting the vacuum tube, 2 collimators for beam shaping, a swiping magnet and several concrete and iron walls for shielding. The main characteristics of the *n\_TOF* neutron beam are the wide energy spectrum, which extends from thermal energy up to several hundred MeV, the very high instantaneous neutron flux, up to 3 orders of magnitude larger relative to previously existing facilities, and the high-energy resolution. All those features make the *n\_TOF* facility very convenient for measuring capture cross-sections of radioactive isotopes, as well as for low-mass samples. The measurements at *n\_TOF* are expected to improve currently available databases, by increasing the accuracy for many isotopes, as well as to provide cross-section data for reactions never measured before.

### 1.1 Physics requirement and motivations

The accuracy of the neutron cross-section measurement is related, among other factors, to the possibility of monitoring the neutron flux with high precision. In particular for capture reactions, data of the sample under investigation have to be compared to a reference measurement, performed for a sample with well known cross sections. In this case, a measurement of the neutron flux for relative normalization becomes

fundamental. At the same time, any device used for the neutron flux determination should present the lowest possible mass, for minimal perturbation of the neutron beam and for minimizing the contribution of background induced by scattered neutrons. At a time-of-flight facility, minimization of all possible background component is of vital importance, since no other method can be applied for background identification and rejection. The accurate determination of neutron cross-sections relies on a precise determination of the neutron flux and its energy dependence. The flux determination can be achieved by measuring the number of protons impinging on the lead target [6] giving an accuracy greater than 1%, too large for our purpose. Moreover, this methods cannot ensure that the same accuracy exists on the neutron flux reaching the sample, due to the possible presence of other effects related to the spallation target or the proton beam optics. A much more reliable information can instead be obtained by measuring the neutron flux in the experimental area, at a relatively small distance from the experimental apparatus. Overall, particular care has to be devoted to minimizing the perturbation of the monitor on the neutron beam and the contribution to the background in the experimental area. Neutron scattered from the material placed in the beam can in fact directly generate spurious hits in the detectors or undergo interactions in the material surrounding it, with the production of  $\gamma$ -rays or secondary neutrons. The effect can be particularly important in the measurement of capture reactions, due to the high sensitivity of the employed detectors to  $\gamma$ -rays. To this respect, it is fundamental to minimize the material present in the beam, since this may significantly increase the amount of scattered neutrons or of secondary particles (in particular  $\gamma$ -rays) produced by neutron interaction with the material inside the experimental area. For this reason, a low mass detector was constructed at *n\_TOF* for monitoring the neutron flux.

### 1.2 Working operation

The device (a schematic sketch of the apparatus is reported in Fig. 1) consists of a thin Mylar foil, with a deposit of  ${}^6\text{Li}$  (or  ${}^6\text{Li}$  compound), inserted in the beam. It allows to monitor the neutron flux from thermal to approximately 1 MeV [7].

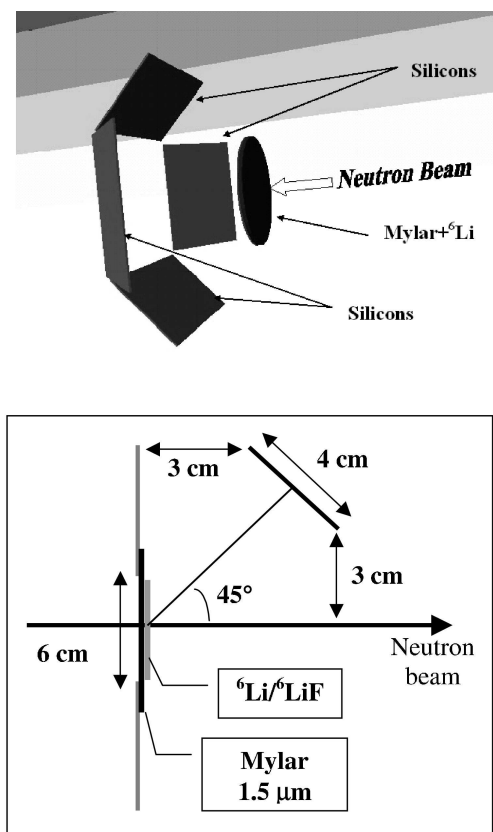


Figure 1. Schematic picture of the neutron flux monitor detector. Upper panel: 3D view of the silicon detectors and the neutron beam. Lower: technical drawing shows the 45 degree position of the silicon detectors and the position of the mylar foil. The  $\alpha$  and tritons produced in the reaction  ${}^6\text{Li}(n, \alpha)t$  are collected in four silicon detectors placed around the neutron beam.

The detection of the tritons and  $\alpha$  particles from the  ${}^6\text{Li}$  capture reaction is performed with an array of Silicon detector placed outside the neutron beam, at a small distance from the foil. In this way, the overall background produced by the flux monitor is related only to the interaction of the neutron beam with the Mylar foil and the  ${}^6\text{Li}$  deposit, both of them relatively thin. The setup operates under vacuum, and is mounted in the experimental area along the neutron beam line. A further minimization of the background induced by scattered neutrons has been achieved by constructing the vacuum chamber in carbon fibre. Silicon detectors of rectangular shape,  $6 \times 4 \text{ cm}^2$ , are placed tangent to a sphere, with the Mylar foil on its center, at a polar angle of 45 degrees.

## 2 The simulations

For a realistic prediction of the triton and  $\alpha$  particle spectrum, the energy resolution of the Si detectors was included in the simulation, using the realistic values for the noise level of few hundred keV. As shown in Fig. 2 for very thin deposit of  ${}^6\text{Li}$ , the  $\alpha$  and the triton peaks are clearly separated. On the other hand, the efficiency corresponding to such a layer of the active deposit is low, and may not be sufficient for

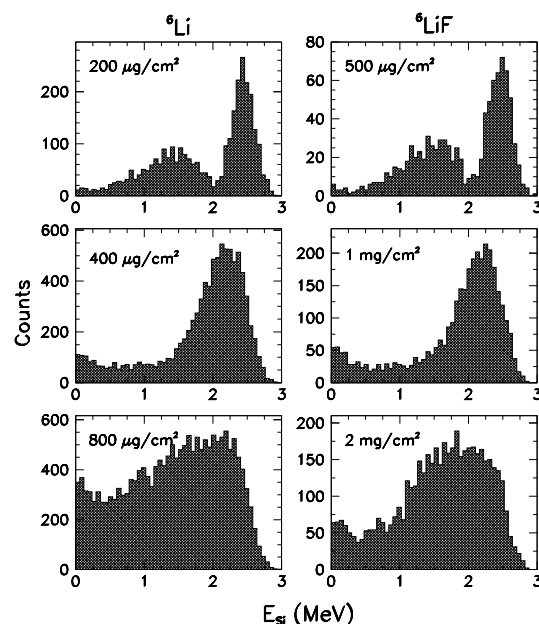


Figure 2. Simulated energy spectrum in the Silicon Detector using different thickness of  ${}^6\text{Li}$  (left column) and  ${}^6\text{LiF}$  (right column) targets. Both the  $\alpha$ -tritons separation and the count rate have to be considered when choosing the optimal target. A resolution of 150 keV has been assumed in the simulations.

some specific applications of the monitor, such as, for example, the precise measurement of the flux in a resonance region. Increasing the thickness of the  ${}^6\text{Li}$  layer, the efficiency increases too, but at the expenses of the resolution, mainly due to the energy loss in the layer itself. Furthermore, for thick layers, a fraction of the  $\alpha$  particles may be stopped inside the deposit. From the simulations, a good triton- $\alpha$  particle separation is observed for thickness up to  $200 \mu\text{g}/\text{cm}^2$  of pure  ${}^6\text{Li}$ . Since  ${}^6\text{Li}$  is highly reactive, and can quickly oxidize when exposed to air, a better choice for the deposit may be represented by a  ${}^6\text{Li}$  compound, such as  ${}^6\text{LiF}$ . Simulations were also performed for this material for comparison. However, the expected count-rate with  ${}^6\text{LiF}$  is lower than for a pure  ${}^6\text{Li}$  layer, for an equivalent  $\alpha$ -triton separation. To minimize the number of scattered neutrons from the hydrogen contents in the mylar foils, a small thickness of  $1.5 \mu\text{m}$  has been used. A Mylar foil  $1.5 \mu\text{m}$  thick is typically used as target of the flux device with a procedure optimized by the target laboratory of the Laboratori Nazionali di Legnaro (hereafter LNL). The procedure consists in making a sandwich of a  ${}^6\text{Li}$  layer between two very thin layers of Carbon, which prevent oxidation at the  ${}^6\text{Li}$ -air interface or at the Mylar- ${}^6\text{Li}$  interface due to the porosity of the Mylar foil. A  $10 \mu\text{g}/\text{cm}^2 \text{C}$  layer seem sufficient for isolating the  ${}^6\text{Li}$  layer from air. First, a layer of C is deposited on the Mylar.  ${}^6\text{Li}$  is then evaporated on the foil, and on top of it a new deposit of C is made. The stability of such a pure  ${}^6\text{Li}$  deposit has been verified over several months of exposure to air. The choice of the Si detectors was based on the need of a large area, low capacitance, low dead-layer and ease of operation. The device chosen is a  $300 \mu\text{m}$  detectors from Micron Semiconductor, with  $6 \times 4 \text{ cm}^2$  area and seven strips (for a course position information). The flux monitor has been mounted and operated at the  $n\text{-TOF}$  facility. A

foil with  $200 \mu\text{g}/\text{cm}^2$  of pure  ${}^6\text{Li}$ , deposited between two layers of  $10 \mu\text{g}/\text{cm}^2$  C was employed in the first measurements. Fig. 2 shows the amplitude distribution of the signals recorded in the Silicon detector. The regions corresponding to the tritons and  $\alpha$ -particles are clearly separated, as expected. For comparison, the prediction of the Monte Carlo simulations, assuming a resolution of 150 KeV, are reported in the figure, showing a remarkable agreement. The part of the spectrum corresponding to the lowest energy  $\alpha$ -particles falls below the threshold, determining a loss of efficiency. Although this can be estimated from the simulations, more accurate results are obtained by concentrating on the analysis of the tritons, which have also the advantage of providing a more precise timing information.

To extract an absolute flux from the Silicon detectors, a correction for the  ${}^6\text{Li}(n, \alpha)t$  cross-section and for the geometric efficiency of the apparatus has to be applied. In following analysis, the ENDF/B-VI database was used for neutron energies up to 1 MeV. The geometric efficiency was estimated by means of the Monte Carlo simulations, performed with the code GEANT3.21. The exact geometry of the foil and of the Si detectors was implemented in the code, as well as the neutron beam profile. The extracted value is approximately 9 % of the total solid angle for a configuration with 4 Si detectors.

### 3 The Carbon fiber scattering chamber and the construction of the device

As already mentioned, a reduction of the background coming from the scatter neutrons captured in the surrounding materials can be obtained by minimizing such material. Since the device has to be hosted in a vacuum chamber we chose carbon fiber as material, since it conjugates the low cross-section of Carbon for neutron interaction with the good mechanical properties of the fiber as structural material. The chamber hosting the device is mounted along the beam line and has to provide a vacuum seal. For this reason, it has been constructed with an inner radius of 20 cm, from 7 to 3 mm thickness, and a length of 60,5 cm. Figure Fig. 3 shows the device mounted at the entrance of the  $n\text{-TOF}$  experimental area, along the neutron beam line.

The foil with the  ${}^6\text{Li}$  deposit, and the Si detectors used for the detection of the products of the reaction  ${}^6\text{Li}(n, \alpha)t$  can be mounted through square flanges built on the cylinder, closed by flat caps hold in place by small clamps. A total of five flanges (two small ones for the foil and two large ones for the Silicon detectors, plus another one for inserting directly a detector in the neutron beam) allow different monitoring systems to be operated simultaneously inside the scattering chamber, whenever it is necessary to maximize the count-rate or to cover different regions of the neutron energy range. Each sector is equipped with a frame for mounting the foil and two frames for the detectors. All frames are mounted on the caps of the flanges, through rails that allow a precise positioning. The detectors can be positioned in

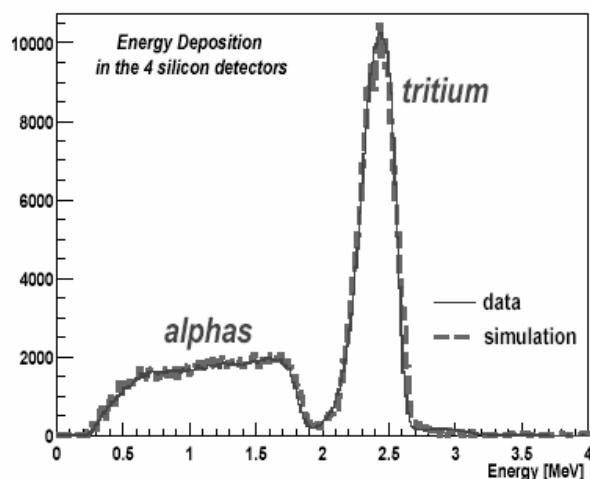


Figure 3. Energy spectrum recorded in the Silicon Detector, obtained from the reconstructed amplitude of the signal digitized with the Flash ADC. For comparison, the prediction of the Monte Carlo simulations are shown in the figure (line).

front and in the back of the foil, thus allowing for coincidence measurements. The Silicon detectors are mounted on a printed copper board, connected to the frame. For each detector, the printed circuit terminates on a LEMO connector mounted on the cap (see Fig. 2). All elements of the scattering chamber, that is the main cylinder, the two flanges, the ports and the frames for the foil and the detectors, are made in carbon fibre. The T800H fabric was used for this purpose, glued together with epoxy resin. To optimize the strength of the chamber and minimize the material, the main body of the chamber was made in one piece only. At the Laboratori Nazionali di Legnaro, the finite element calculations have been made, and all molds has been constructed, while the lamination of the fiber has been performed by an external company (RI-BA, Faenza, Italy). During the construction, a copper socks was embedded in the texture of the vacuum chamber, to improve the noise shielding of the Silicon detectors. A vacuum leakage of  $10^{-7} \text{mbar} \cdot \text{l/s}$  has been achieved even though large flanges and large surfaces were employed, reaching the limit of the viton o-ring seals. The final density of the material was estimated to be  $1.92 \text{g}/\text{cm}^3$ . To perform accurate simulations, an accurate determination of the composition is needed, so that we performed an RBS analysis. The following ratio for the most abundant elements was found: C : O : N : Ca : Br = 2 : 0.2 : 0.16 : 0.012 : 0.016. No information were available about Hydrogen content, but the amount can be roughly estimated from the amount of Oxygen yielding a ratio: H/O=7,5  $1022 \text{ (atoms}/\text{cm}^3)$  /  $1,2 \cdot 1022 \text{ (atoms}/\text{cm}^3)$ . The thickness of the chamber was chosen so to withstand a pressure of 7 bars, a tolerance required by CERN for safety reasons. Compared to the requests for Aluminium, the safety issue results in a slightly thicker chamber. However, given the larger density of the Aluminium, and the higher average capture cross-section, the use of carbon fibre results in a reduction of approximately 1/3 in weight, and much more in terms of induced background (see figure Fig. 4).

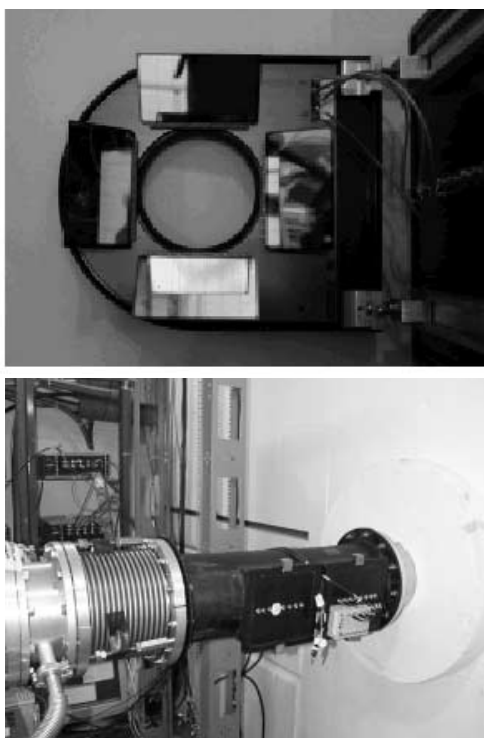


Figure 4. Upper panel: View of the detector sector placed on the largest square flanges (see lower panel). Here the silicon detectors are visible, together with the 50 ohmm adapted printed circuit and the LEMO connectors. Lower: view of the entrance of the beam line, where the flux monitor detector has been mounted. Two large flanges host the LEMO connectors (see upper panel) which give out the connections of the detectors placed inside the chamber. The external box hosts the preamplifiers.

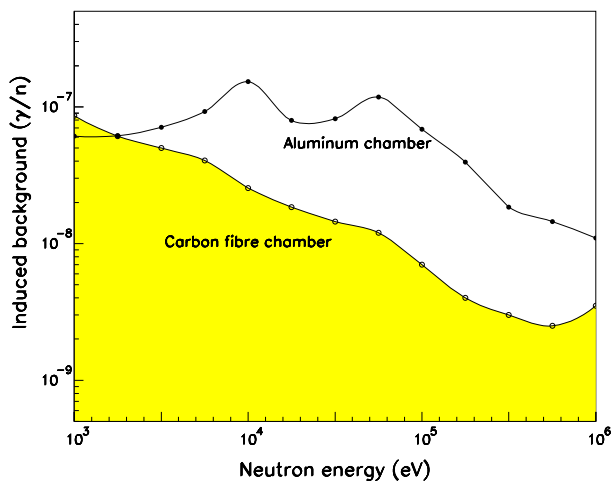


Figure 5. Results of the simulation of the induced background for a vacuum scattering chamber made of Carbon Fiber (CF) and Aluminum. the comparison shows the clear advantage of using CF even if a safety coefficient 7 was used (see text).

The internal electrical layout between the detectors (inside the chamber) and the preamplifier (a box outside) are very important to reduce the noise. A good results was obtained by making an 50 ohmm adapted printed circuit that can hold the detectors, and transfer the signal from them to the flange where the preamplifier are mounted by using 50 Ohm adapted tracks (see upper part of figure Fig. 5).

## 4 Conclusions

A low-mass neutron flux detector has been set-up to monitor the neutron beam at the new  $n\_TOF$  facility at CERN. The main features of the device are the minimal perturbation of the beam and of the induced background. This has been achieved by inserting in the neutron beam only a thin Mylar foil with a  ${}^6Li$  (or a  ${}^6Li$ -compound) and using carbon fiber as constructive material. An array of Silicon detectors, used for recording the charged products of the  ${}^6Li(n, \alpha)t$  reaction, is placed outside the beam around the foil. In a setup with 4 detectors, a geometric efficiency higher then 10 % is achieved when analyzing only tritons. The chamber allows for several monitoring sectors to be operated simultaneously. A particular procedure has been used to evaporate a pure  ${}^6Li$  deposit that remains stable even when exposed to air for several weeks. The flux monitor here described has been mounted inside the  $n\_TOF$  experimental area and operated in the first measurement campaign. The device has been used in the measurements of capture reactions, for the neutron beam characterization, as well as in the first campaign of dedicated measurements.

## References

- [1] C. Rubbia et al., CERN/AT/95-44, CERN (1995);
- [2] C.D. Bowman, Ann. Rev. Nucl. Part. Sci. **48**, 505 (1998).
- [3] For an ADS review see the Proceedings of "6th Information Exchange Meeting on Actinide and Fission Product and Partitioning Transmutation" Madrid 11-13 December 2000;
- [4] F. Köppler, F.K. Thielemann, and M. Wiescher, Ann. Rev. Nucl. Part. Sci. **48**, 175 (1998).
- [5] The  $n\_TOF$  Collaboration, "Proposal for a neutron time-of-flight facility", CERN-SPSS 99-08, SPSC-P310, March 1999.
- [6] The  $n\_TOF$  Collaboration, "n - TOF Technical Report", CERN-INTC 2000-018, CERN (2000).
- [7] "Nuclear Data Standards for Nuclear Measurements", NE-ANDC - 311 U, INDC(SEC)-101, 1992;